Delay interferometric single-shot measurement of a petawatt-class laser longitudinal chromatism corrector

C Rouyer, N Blanchot, Jérôme Neauport, C Sauteret

Delay interferometric single-shot measurement of a petawatt-class laser longitudinal chromatism corrector

C. Rouyer, N. Blanchot and J. Neauport

Commissariat à l'énergie atomique, Centre d'études scientifiques et techniques d'Aquitaine, BP 2, 33114 Le Barp, France
claude.rouyer@cea.fr

C. Sauteret

Laboratoire pour l'Utilisation des Lasers Intenses, UMR 7605, Ecole Polytechnique, 91128 Palaiseau, France

Abstract: In this paper we present a self-referenced interferometric single-shot measurement technique that we use to evaluate the longitudinal chromatism compensation made by a diffractive lens corrector. A diffractive lens with a delay of 1 ps is qualified for a 60 mm beam aperture. This corrector was implemented on the Alisé Nd:glass power chain. We qualify the corrector and the Alisé power chain chromatism, demonstrating the potential of this measuring principle as well as the interest of diffractive lenses to correct longitudinal chromatism of petawatt-class lasers.

OCIS codes: (140.7090) Lasers and laser optics: Ultrafast lasers; (050.0050) Diffraction and gratings: diffraction and gratings; (220.1000) Optical design and fabrication: aberration compensation

References and links

1. C. Cavailler, N. Fleurot, T. Lonjaret, and J. M. Di-Nicola, "Prospects and progress at LIL and Megajoule," Plasma Phys. Controlled Fusion **46**, B135-B141 (2004).
2. B. M. Van Wonterghem, S. C. Burkhart, C. A. Haynam, K. R. Manes, C. D. Marshall, J. E. Murray, M. L. Spaeth, D. R. Speck, S. B. Sutton, and P. J. Wegner, "National Ignition Facility commissioning and performance," Proc. SPIE **5341**, 55-65 (2004).
3. N. Blanchot, E. Bignon, H. Coïc, A. Cotel, E. Couturier, G. Deschaseaux, N. Forget, E. Freysz, E. Hugonnot, C. LeBlanc, N. Loustalet, J. Luce, G. Marre, A. Migus, S. Montant, S. Mousset, S. Noailles, J. Néauport, C. Rouyer, C. Rullière, C. Sauteret, L. Videau, and P. Vivini, "Multi – Petawatt High Energy Laser Project on the LIL Facility in Aquitaine," Proc. SPIE **5975**, 30 (2005).
4. D. Strickland and G. Mourou, "Compression of amplified chirped optical pulses," Opt. Commun. **56**, 219-221 (1985).
5. N. Blanchot, G. Marre, J. Neauport, E. Sibe, C. Rouyer, S. Montant, A. Cotel, C. Le Blanc, and C. Sauteret, "Synthetic aperture compression scheme for multi-Petawatt high energy laser," Appl. Opt. **45**, 1-8 (2006).
6. L. J. Waxer, D. N. Maywar, J. H. Kelly, T. J. Kessler, B. E. Kruschwitz, S. J. Loucks, R. L. McCrory, D. D. Meyerhofer, S. F. B. Morse, C. Stoeckl, and J. D. Zuegel, "High-energy Petawatt capability for the Omega laser," Opt. Photon. News **16**, 30 (2005).
7. C. P. J. Barty, M. Key, J. Britten, R. Beach, G. Beer, C. Brown, S. Bryan, J. Caird, T. Carlson, J. Dawson, A. C. Erlandson, D. Fittinghoff, M. Hermann, C. Hoaglan, A. Iyer, L. Jones II, I. Jovanovic, A. Komashko, O. Landen, Z. Liao, W. Molander, S. Mitchell, E. Moses, N. Nielsen, H-H. Ngyuen, J. Nissen, S. Payne, D. Pennington, L. Risinger, M. Rushford, K. Skulina, M. Spaeth, B. Stuart, G. Tietbohl, and B. Wattellier, "An overview of LLNL high-energy short-pulse technology for advanced radiography of laser fusion experiments," Nucl. Fusion **44**, S266-S275 (2004).
8. C. Le Blanc, C. Felix, J. C. Lagron, N. Forget, Ph. Hollander, A. M. Sautivet, C. Sauteret, F. Amiranoff, and A. Migus, "The petawatt laser glass chain at LULI: from the diode-pumped front end to the new generation of compact compressors," in *Proceedings of Third International Conference on Inertial Fusion Sciences and Applications*, B. A. Hammel, D. D. Meyerhofer, J. Meyer ter Vehn, and H. Azechi, eds., (American Nuclear Soc. Inc, La Grange Park, IL, USA, 2004), pp. 608-611.
9. C. N. Danson, P. A. Brummitt, R. J. Clarke, J. L. Collier, B. Fell, A. J. Frackiewicz, S. Hancock, S. Hawkes, C. Hernandez-Gomez, P. Holligan, M. H. R. Hutchinson, A. Kidd, W. J. Lester, I. O. Musgrave, D. Neely, D. R. Neville, P. A. Norreys, D. A. Pepler, C. J. Reason, W. Shaikh, T. B. Winstone, R. W. W.

#78030 - $15.00 USD Received 12 December 2006; revised 17 January 2007; accepted 17 January 2007

Wyatt, and B. E. Wyborn, "Vulcan Petawatt-an ultra-high-intensity interaction facility," Nucl. Fusion **44**, S239-S246 (2004).
10. K. Mima, H. Azechi, Y. Johzaki, Y. Kitagawa, R. Kodama, Y. Kozaki, N. Miyanaga, K. Nagai, H. Nagatomo, M. Nakai, H. Nishimura, T. Norimatsu, H. Shiraga, K. Tanaka, Y. Izawa, Y. Nakao, H. Sakagami, "Present status of fast ignition research and prospects of FIREX project," Fusion Sci. Technol. **47**, 662 (2005).
11. M. Martinez, E. Gaul, T. Ditmire, S. Douglas, D. Gorski, W. Henderson, J. Blakeney, D. Hammond, M. Gerity, J. Caird, A. Erlandson, I. Iovanovic, C. Ebbers, B. Molander, "The Texas Petawatt Laser," Proc. SPIE **5991** (Feb. 7, 2006).
12. J. D. Zuegel, S. Borneis, C. Barty, B. Le Garrec, C. Danson, N. Miyanaga, P. K. Rambo, C. Le Blanc, T. J. Kessler, A. W. Schmid, L. J. Waxer, J. H. Kelly, B. Kruschwitz, R. Jungquist, E. Moses, J. Britten, I. Jovanovic, J. Dawson, and N. Blanchot, "Laser Challenges for Fast Ignition," Special Issue on Fast Ignition, Fus. Sci. Technol. **49**, 453 (2006).
13. Z. Bor, "Distortions of femtosecond laser pulses in lens systems," J. of Modern Opt. **35**, 1907-1918 (1988).
14. J. Néauport, N. Blanchot, C. Rouyer and C. Sauteret, "Chromatism compensation of the PETAL multi-petawatt high energy laser," Appl. Opt. (to be published).
15. R. Netz, T. Feuer, R. Wolleschensky, R. Sauerbrey, "Measurement of the pulse-front distortion in high-numerical-aperture optics," Appl. Phys. B **70**, 833-837 (2000).
16. G. Petzler, A. Kasper, K. J. Witte, "Angular chirp and tilted light pulses in CPA lasers," Appl. Phys. B **70**, 1-9 (2000).
17. H.-M. Heuck, P. Neumayer, T. Kühl, U. Wittrock, "Chromatic aberration in Petawatt class laser," Appl. Phys B **84**, 421-428 (2006).
18. H. Kogelnik and T. Li, "Laser beams and Resonators," Appl. Opt. **5**, 1550-1567 (1966).
19. Z. Bor, "Distortion of femtosecond laser pulses in lenses," Opt. Lett. **14**, 119- (1989).
20. http://www.llnl.gov/nif/psa/diffractive-optics/fresnel.html.
21. N. Blanchot, J. Néauport, C. Rouyer and C. Sauteret, "Chromatism compensation of the PETAL multi-petawatt high energy laser," in proc. of International Conference on Ultrahigh Intensity Laser (ICUIL), p211, Cassis, 24-29 September 2006.
22. N. Blanchot, D. Le Goff, I. Le Goff, P. Manac'h, E. Mazataud, M. Nicolaizeau, M. Padois, L. Videau, D. Villate, L. Voisin, "A new versatile Nd:glass 200 J facility: ALISE; or from monochromatic and smoothed nanosecond pulses towards the ultra-intense femtosecond regime," in *Conference on Lasers and Electro-Optics/International Quantum Electronics Conference*, Technical Digest (Optical Society of America, 2002), paper CWB4, 364-365.
23. http://www.silios.com.
24. J. Neauport, E. Journot, G. Gaborit and P. Bouchut, "Design, optical characterization and operation of large transmission gratings for the laser integration line and laser megajoule facilities," Appl. Opt. **44**, 3143-3152, (2005).

1. Introduction

Ignition scale facilities now under construction, the LMJ [1] (*Laser MégaJoule*, in France) and the NIF [2] (*National Ignition Facility*, in the USA), constitute a remarkable opportunity in science and for inertial confinement fusion applications. The LIL, the LMJ laser prototype consists of an elementary unit of the LMJ, equipped with eight beams. Each beam is able to deliver a nanosecond pulse of 18 kJ at the fundamental wavelength of 1.053 µm and 7 kJ on target at 351 nm. The LIL facility will be split into eight independent beams to obtain a symmetrical irradiation on target. Moreover, an additional laser line, called PETAL (PETawatt Aquitaine Laser), offering multi-petawatt, high energy capabilities is currently being constructed [3].

The PETAL facility is designed to deliver an energy of 3.6 kJ in 500 fs at the wavelength of 1.053 µm. It is based on the Chirped Pulse Amplification (CPA) technique [4] and uses a synthetic aperture compression scheme detailed previously [5]. PETAL, such as any other high energy Petawatt project (Omega-EP [6], NIF-ARC [7], PICO2000 [8], VULCAN [9], FIREX [10] or the Texas Petawatt Laser [11], uses a series of spatial filters in its amplifier section to extend, image-relay and clean the laser beam of unwanted spatial frequency modulations. These spatial filters, formed with a pair of lenses, introduce longitudinal chromatism and thus temporal delay. If this effect can be neglected for nanosecond regime lasers, it becomes a crucial issue for short pulses [12] and has consequently to be corrected. Many solutions, from classical achromats to diffractive optics [11-13], exist to compensate this longitudinal chromatism. The PETAL corrector, called CROCO (ChROmatism

#78030 - $15.00 USD Received 12 December 2006; revised 17 January 2007; accepted 17 January 2007

COrrector), takes benefit of the inverse chromatism of a diffractive optic with respect to a transparent material [14].

In order to validate the chromatic correction, we need an accurate measurement of the spatial dependence of the pulse delay induced by the longitudinal chromatic aberrations in the power chain as well as the one induced by the corrector component. Several methods have been proposed using a reference pulse [15]. These methods are based on spatial interferometry, spectral interferometry or autocorrelation processes. "Inverted field autocorrelation" [16] is a measurement without a reference pulse. Its extension, "shifted field autocorrelation" [17], with a spatial shift in one interferometer arm limits the interference pattern in the overlapping region of the two pulses. However, all these methods require multiple shots to estimate the delay inside the beam. We herein present an extension of the spectral interferometry technique using the principle of the shifted arm to realize a 2D-spectral interferometry allowing the measurement of the pulse delay with a single shot. Moreover, this technique does not require an unaberrated mutually coherent simultaneous reference beam to interfere with the test beam.

We therefore propose to experimentally measure the delay compensation introduced by the CROCO using a single shot technique. The experimental setup consists of an interferometer coupled with a spectrometer to give access to the CROCO's induced delay. The second section of this paper recalls the total delay introduced by the amplifier section of the PETAL facility and details the CROCO system. Section 3 is devoted to experimental measurements. After a description of the corrector manufacturing and the optical characterisation, we detail the experimental setup and the physical principles of the delay measurement. We then conclude by the obtained experimental delay to show that it is in good agreement with the CROCO specifications.

2. Evaluation and correction of the longitudinal chromatism for the PETAL facility

We analyzed in a previous work the global chromatism of the amplifier section of the PETAL facility and the various solutions to compensate it [14]. For the sake of completion, we would like to detail the various approaches existing to understand, represent and quantify the longitudinal chromatism.

Let's consider a single lens presenting some chromatism, its focal length variation with the wavelength can be expressed as, at the first order:

$$f(\lambda) = f_0 + \dot{f} \cdot (\lambda - \lambda_0) \tag{1}$$

Where f_0 is the focal length at central wavelength λ_0 and $\dot{f}$ is the derivative of the function f with respect to the wavelength λ.

We can then define a value ΔZ which is characteristic of the amount of chromatism obtained for a spectral bandwidth of $\Delta\lambda$:

$$\Delta Z = \dot{f} \cdot \Delta\lambda \tag{2}$$

This chromatism can be also expressed as the phase difference $\Delta\phi$ of the wavefront, on the edges of the pupil and of the spectrum. This phase shift characteristizes a defocusing of the beam:

$$\Delta\phi = \frac{2\pi}{\lambda_0} \cdot \frac{h^2}{f_0^{\,2}} \cdot \frac{\Delta Z}{2} \tag{3}$$

Let's define Z_R, the Rayleigh length [18]:

$$Z_R = A \cdot \frac{f_0^{\,2} \lambda_0}{h^2} \tag{4}$$

Where A is a form factor close to unity and h is the radius of the pupil.

#78030 - $15.00 USD Received 12 December 2006; revised 17 January 2007; accepted 17 January 2007

From Eqs. (3) and (4) we obtain the expression of the phase difference induced by the chromatism for a spectral bandwidth $\Delta\lambda$:

$$\Delta\phi = \pi \cdot \mathrm{A} \cdot \frac{\Delta \mathrm{Z}}{\mathrm{Z_R}} \tag{5}$$

The chromatic aberration can also be described, for the central wavelength λ_0, by the optical path length difference and defined by $\Delta\phi = 2\pi \cdot \frac{\Delta}{\lambda_0}$:

$$\frac{\Delta}{\lambda_0} = \frac{\Delta\phi}{2\pi} = \frac{\mathrm{A}}{2} \cdot \frac{\Delta \mathrm{Z}}{\mathrm{Z_R}} \tag{6}$$

Note that here the chromatism is proportional to the spectral bandwidth. From a temporal point of view, the chromatism can be seen as the time delay T_d between the rays propagating through respectively the edges and the center of the pupil. Hence, Z. Bor [19] and H. M. Heuck [17] demonstrated that:

$$\mathrm{T_d} = \frac{\lambda_0}{2\mathrm{c}} \cdot \frac{\mathrm{h}^2}{\mathrm{f_0}^2} \cdot \dot{\mathrm{f}} \tag{7}$$

From Eqs. (2) and (4), we deduce that:

$$\mathrm{T_d} = \frac{\lambda_0^{\,2}}{\Delta\lambda} \cdot \frac{\mathrm{A}}{2\mathrm{c}} \cdot \frac{\Delta \mathrm{Z}}{\mathrm{Z_R}} \tag{8}$$

If we now introduce the Fourier limited pulse length associated with the spectral width $\Delta\nu$:

$$\tau \cdot \Delta\nu = \mathrm{B} \tag{9}$$

where B is a form factor close to unity and τ is the pulse duration. Hence, the delay T_d characteristizing the chromatism can be written as:

$$\frac{\mathrm{T_d}}{\tau} = \frac{\mathrm{A}}{2\mathrm{B}} \cdot \frac{\Delta \mathrm{Z}}{\mathrm{Z_R}} \tag{10}$$

In consequence, we conclude that both temporal and spectral descriptions lead to an expression of the chromatism with the same adimensioned ratio. This ratio is algebraic and is cumulative at the traversing of a succession of lenses.

$$\frac{\Delta}{\lambda_0} = \frac{\Delta\phi}{2\pi} = \frac{\mathrm{A}}{2} \cdot \frac{\Delta \mathrm{Z}}{\mathrm{Z_R}} = \mathrm{B} \cdot \frac{\mathrm{T_d}}{\tau} \tag{11}$$

These two temporal and spectral descriptions of the chromatism are depicted on Fig. 1.

#78030 - $15.00 USD Received 12 December 2006; revised 17 January 2007; accepted 17 January 2007

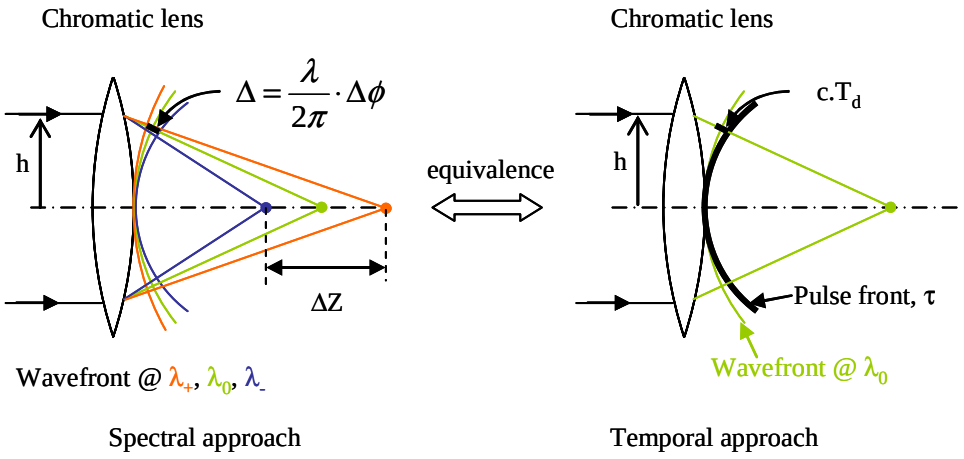

Fig. 1. Description of various characteristic quantities of the chromatism brought by a lens. Δ is the optical path length difference and ΔΦ is the phase difference on the border of the pupil h and for a spectral bandwidth $\Delta\lambda=\lambda_+-\lambda_-$. ΔZ is the defocusing for the same spectral bandwidth and T_d the time delay between centre and border of the pupil. Both approaches depict the same chromatism phenomenon.

To measure the chromatism, we thus need an experimental setup enabling us to estimate this ratio. As described in section 3, the temporal approach is used for our measurements. As explained above, the same work can be made in the spectral domain leading to the same conclusion.

For the PETAL facility, the four pass amplifier section uses 6 lenses of various foci and radii so that the total induced delay is equal to 1520 fs i.e. about 3 times the PETAL expected pulse duration. The effect of a 2 ps additional delay on the focal spot on target for a flat top square beam can be numerically predicted and is illustrated in Fig. 2 [3]. We can see that the peak intensity is divided by 8 in absence of chromatism correction.

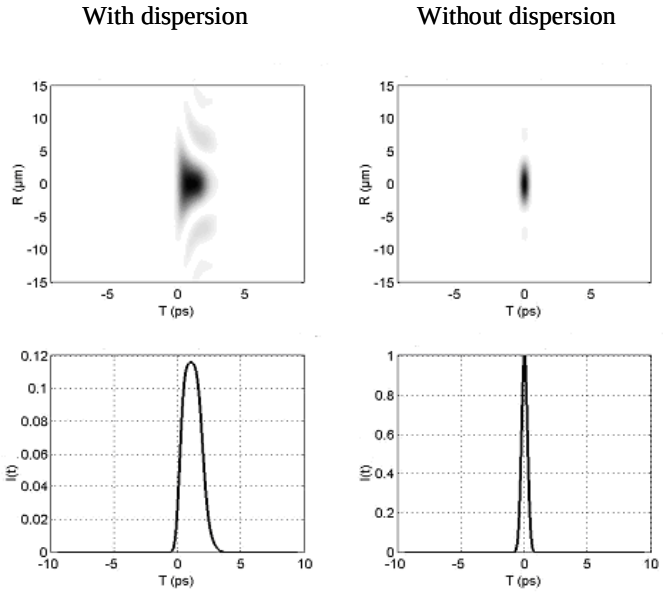

Fig. 2. Effect of longitudinal chromatism on peak intensity on target for the PETAL facility. Left: with longitudinal chromatism, Right: without longitudinal chromatism, Top: focal spot radius evolution versus time. Bottom: central focal spot intensity versus time.

#78030 - $15.00 USD Received 12 December 2006; revised 17 January 2007; accepted 17 January 2007

Several methods can be proposed to compensate the longitudinal chromatism [11, 13, 14, 17]. Due to the significant amount of pulse delay to be corrected and the laser line architecture, a diffractive based solution has been retained for the PETAL facility [14]. We have demonstrated that a focusing grating with an edge line density of N = 12.767 l/mm is adequate to compensate the 1520 fs delay, this corresponds to a 2.523 m diffractive lens. Such a low line density focusing grating would exhibit very low diffraction efficiency. Therefore, a diffractive Fresnel lens was preferred. It consists of a Fresnel lens with a binarized one wave deep profile. Using a four-mask manufacturing process, the 16 level diffractive Fresnel lenses can exhibit a theoretical diffraction efficiency of 98.5% [20]. Implementation of a CROCO in the L-turn of the PETAL amplifier section is done by placing a null power optical system constituted of the diffractive corrector and of a diverging lens in front of the L-turn mirror (M2) as illustrated in Fig. 3.

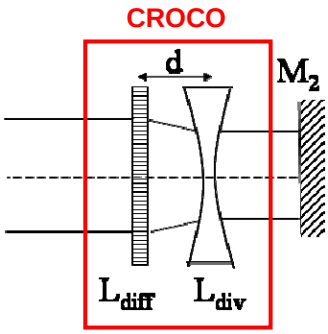

Fig. 3. The CROCO system in front of the M2 (L-turn) mirror. L_{diff} is the diffractive lens, L_{div} is the diverging lens. The (L_{diff}-L_{div}) ensemble has a null power.

It can be noticed that if this null power corrector is placed in a diverging or converging beam, a simple translation of the CROCO modifies the number of grooves on the diffractive lens overlapped by the beam and therefore the degree of correction of the system. A patent is currently pending on this tunable chromatism corrector.

Based on an early design, the work detailed in this paper is done with a 1.5 m diffractive lens, instead of the 2.523 m lens specified for PETAL. It has no impact on the announced conclusion.

3. Experimental demonstration

3.1 Experimental set-up: interferometric single shot chromatism measurement

We herein detail the experimental set-up allowing the measurement of the delay compensation introduced by the CROCO. Compared to other measurements [15, 17], we propose an interferometric single-shot technique. Our diagnostic is based on a 2D-spectrally resolved interferometer [21]. An interferometer using two dihedrons generates two replicas of the beam shifted in transverse space and delayed in time. The overlapping region of the two replicas is analysed by a spectrograph. The spatial shift is made along the slit of the spectrograph. As shown in Fig. 4, temporal delay produces spectral interference in the overlapping region and perpendicularly to the slit. A spatial variation of the delay along the slit (Y direction) will then induce a variation of the fringe period. The temporal delay is adjusted to obtain about ten fringes in order to use 1D-Fourier transform analysis in the spectral domain. As explained in the next paragraph, it is the 1D-FFT satellite positions that give access to the delay for each spatial Y-coordinate.

#78030 - $15.00 USD Received 12 December 2006; revised 17 January 2007; accepted 17 January 2007

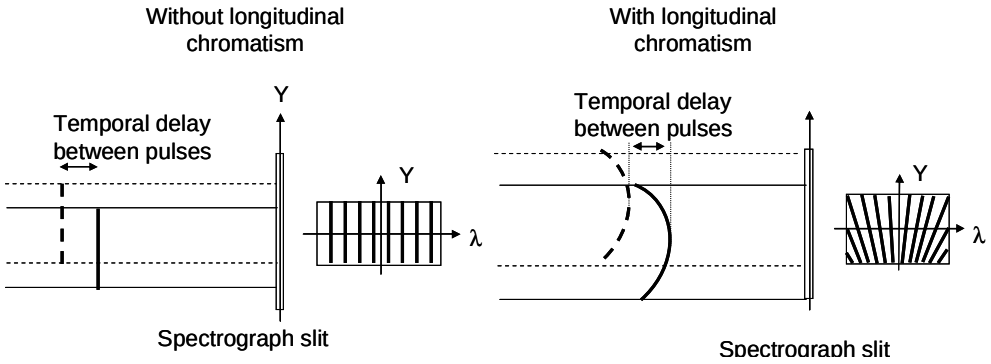

Fig. 4. Spectral interferences observed on the spectrograph. Left: regular fringes in the case of constant delay between the two replicas. Right: variation of the fringes frequency in the case of chromatic beam.

The electric fields of two replicas delayed by T = 2 Δt are, in the spectral domain:

$$E_1(\omega) = A(\omega)exp(i\omega\Delta t) \tag{12}$$

and

$$E_2(\omega) = A(\omega)exp(-i\omega\Delta t) \tag{13}$$

At the output of the spectrograph, the total electric field is given by:

$$E(\omega) = E_1(\omega) + E_2(\omega) = 2A(\omega)cos(\omega\Delta t) \tag{14}$$

and its intensity is:

$$I(\omega) = E(\omega)E^*(\omega) = 2A(\omega)\cdot A^*(\omega)[cos(2\omega\Delta t) + 1] \tag{15}$$

The period p of the cosine has the following property:

$$p = \frac{\pi}{\Delta t} = \frac{2\pi}{T} \tag{16}$$

The relation between the temporal width τ_o and the spectral bandwidth Δω is given by $\tau_0\Delta\omega = 2\pi\cdot B$. The number of visible fringes N in the spectrum Δω is N=Δω/p and is defined by:

$$N = B\cdot\frac{T}{\tau_0} \tag{17}$$

Let us consider a longitudinal chromatic beam such as depicted in Fig. 5, its energy front is curved and its temporal delay depends on the spatial coordinate Y:

$\tau(y) = T_r\left(\frac{y}{a}\right)^2$, where a is the radius of the beam and T_r the delay between the centre and the edge of the beam.

#78030 - $15.00 USD Received 12 December 2006; revised 17 January 2007; accepted 17 January 2007

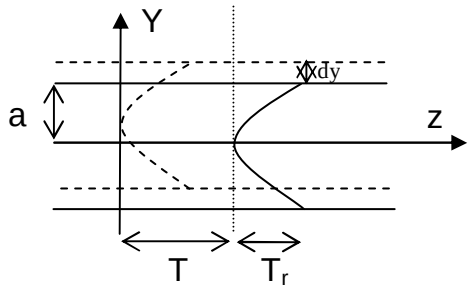

Fig. 5. Spatial shift dy in the case of a chromatic beam having a temporal delay T between the two replicas. T_r is the chromatic temporal delay.

For a spatial shift dy, the delay between two replicas is:

$$\Delta\tau = \tau(y) + T - \tau(y - dy) = T_r \frac{2ydy}{a^2} + T - T_r \frac{dy^2}{a^2} \tag{18}$$

The maximum delay variation, giving the maximum variation of the number of fringes, is obtained for a spatial shift equal to the beam radius: dy = a. Under this condition, the delay is:

$$\Delta\tau = T + T_r \frac{2y}{a} - T_r \tag{19}$$

The maximum delay is obtained for y = a given $\Delta\tau(y = a) = T + T_r$, and the minimum delay for y = 0 given $\Delta\tau(y = 0) = T - T_r$.

So, the number of fringes defined in Eq. (17) increases linearly because of the shift:

$$N_{min} = B \cdot \frac{T - T_r}{\tau_0}\,;\; N_{max} = B \cdot \frac{T + T_r}{\tau_0}\,;\; \Delta N = N_{max} - N_{min} = B \cdot \frac{2T_r}{\tau_0} \tag{20}$$

The experiments presented here were made on the Alisé facility [22] at the CEA-CESTA. This facility is able to deliver nanosecond to femtosecond pulses at an energy ranging from a millijoule to a few hundred joules. In these experiments, chirped pulse capability is used. Pulses, generated by a Mira oscillator are stretched up to 1.7 ns (16 nm) and amplified in a Ti:sapphire regenerative cavity up to 2 mJ. The spectrum is reduced to 7 nm because of gain narrowing. The beam propagates through the power chain increasing its diameter up to 85 mm. The amplification section is not activated. We only use the magnification factor of the chain to implement the diffractive lens (see § 3.2.) specified to produce a delay of T_r = 1 ps for a 60 mm diameter. After propagating through the diffractive lens, the Alisé beam size is reduced before the interferometer down to a 1 cm beam diameter. One replica is delayed of 5 ps and the second replica is spatially shifted of half the beam size based on previous considerations. An imagery telescope is inserted to image the diffractive lens plane on the spectrograph slit to avoid spatial distortions (versus wavelength) due to the chromatism. Moreover the slit has to be adjusted to be parallel to the shearing direction. Using Alisé characteristics, the 5 ps delay will create 10 fringes on the spectrograph. The additional 1 ps delay of the diffractive lens, on the edge of the overlapping zone, will increase the fringe number from 10 to 12. The experimental set-up is detailed in Fig. 6. The diffractive lens can be replaced by a refractive lens to give access to both the longitudinal chromatisms of the diffractive lens and of the Alisé power chain.

#78030 - $15.00 USD Received 12 December 2006; revised 17 January 2007; accepted 17 January 2007

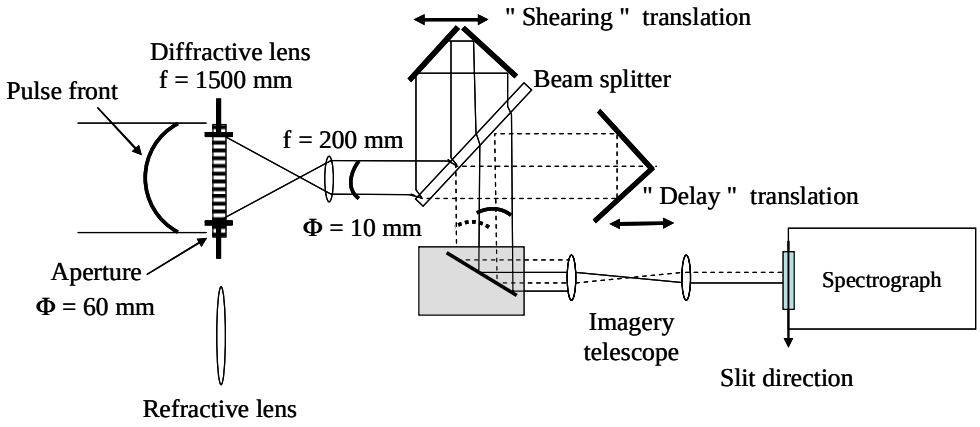

Fig. 6. Experimental set-up used on the Alisé facility to realize a single shot measurement of the chromatism induced by a diffractive lens.

3.1. Diffractive Fresnel lens specifications and optical performances

A 1.5 m diffractive lens was manufactured by the SILIOS Company [23] using a multi-mask dry etching process with the following specifications. This lens induces a 1 ps delay. A photo of the manufactured component is given in Fig. 7:

Substrate material: Corning 7980 fused silica
Full size: 100 mm -0.1/-0.4 mm
Clear aperture: 60x60 mm²
Thickness: 8 mm +/-0.1 mm
Parallelism: <1"
Substrate form: plane-plane
Transmitted wavefront quality before Fresnel lens engraving: <λ/10 @ 1.053µm
Side A and B planarity before Fresnel lens engraving: <λ/5 @ 1.053µm
Fresnel lens etched on side A, focal length of 1.5 m
Fresnel lens maximal depth: λ/(n-1) @ 1.053µm where n is the index of fused silica at this wavelength
Fresnel lens profile binarized on 16 levels
No antireflection coating on sides A and B

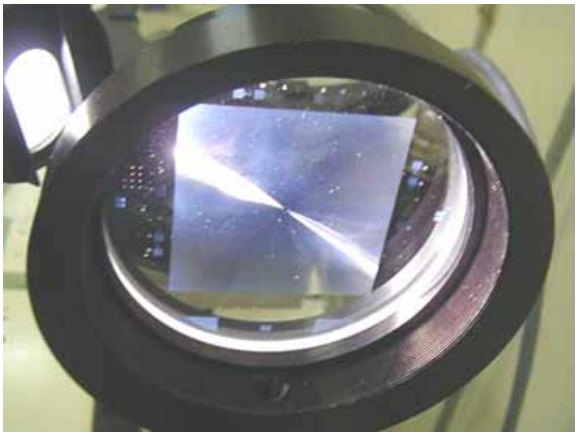

Fig. 7. Picture of the diffractive lens (SILIOS Company) used in these experiments.

#78030 - $15.00 USD Received 12 December 2006; revised 17 January 2007; accepted 17 January 2007

The diffraction efficiency of this lens was measured on a specific photometer. This device was previously described [24]. It consists of a single point scanning system with a 5 mm diameter beam of that can operate at 351 nm, 523 nm or 1053 nm at variable incidence angles. The estimated absolute accuracy of the apparatus is ± 0.0015. The first transmitted order diffraction efficiency was measured at normal incidence on the clear aperture with a sampling step of 4.3 mm x 4.3 mm. The obtained result is given in Fig. 8.

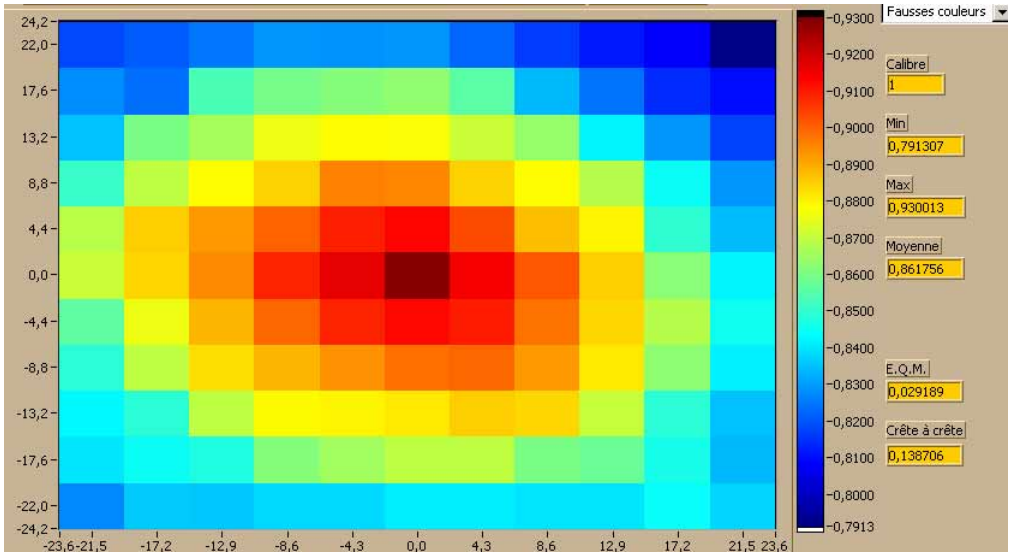

Fig. 8. Diffraction efficiency of the 1.5 m Fresnel lens at 1053 nm, normal incidence.

If we take into account the 4% losses of the uncoated side, a mean diffraction efficiency of 0.897 is obtained. A maximal value of 0.9672 is measured at the centre of the part, which is close to the theoretical maximal value for a 16 level part of 0.985. Fall off of the diffraction efficiency in the corner is due to the reduction of the size of the Fresnel lens pattern. The theoretical pattern in the corner is probably not respected by the manufacturing process.

3.2. Experimental results

As explained in section 3.1., the experiment consists of two series of measurements to observe variations of the interference pattern. The analyses of these measurements with a Fourier transformation technique are detailed after.

A first measure is made with a refractive lens instead of the diffractive lens. This is a kind of a reference for the qualification of the diffractive lens. Indeed, in this case, the accumulated chromatism is the sum of both the Alisé power chain chromatism and the diagnostic chromatism *i.e.* the refractive lens, the second lens of the telescope and the imagery telescope (see Fig. 6). As shown in Fig. 9, the period of the obtained interference pattern is quasi-constant on the full image. The global distortion of the fringes is due to wavefront aberrations of the input beam. In a future paper, we will demonstrate how an adequate use of this specific pattern can also give access to spectrally resolved wavefront aberrations in the manner of a large bandwidth shearing interferometer.

#78030 - $15.00 USD Received 12 December 2006; revised 17 January 2007; accepted 17 January 2007

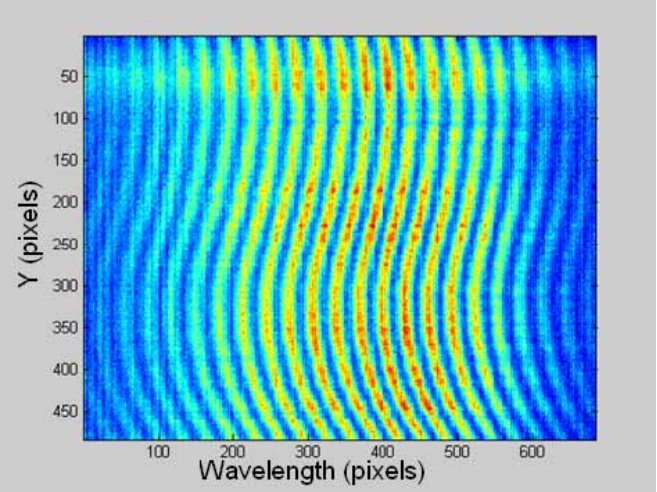

Fig. 9. Experimental interference pattern with the classical refractive lens. The interference period seems to be quasi-constant on the whole image. The horizontal axis is the wavelength axis in CCD pixel numbers. The vertical axis is the transverse coordinate axis along the spectrograph slit in CCD pixel numbers.

In the second series of measurements, the refractive lens is replaced by the diffractive lens described in section 3.2. Due to the variation of the delay between the top and the bottom of the overlapping zone, we observe in Fig. 10 a variation of the period of the interference pattern. The cut-off in the spatial profile comes from the limited size of the diffractive lens with a 60 mm aperture.

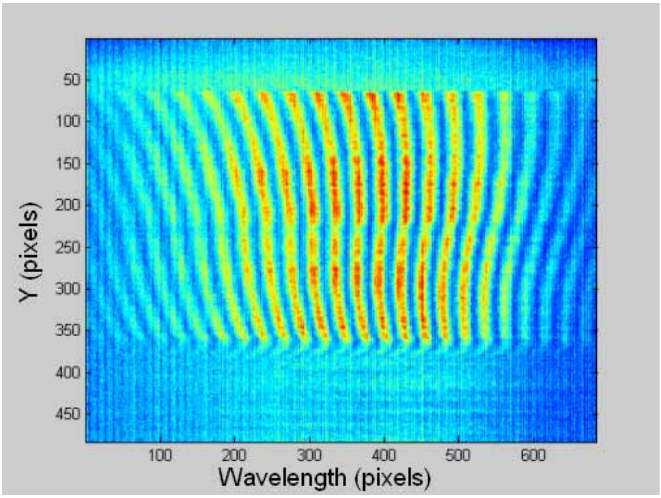

Fig. 10. Experimental interference pattern with the diffractive lens. A variation of the interference period is clearly observable between the top and the bottom of the image. The horizontal axis is the wavelength axis in CCD pixel numbers. The vertical axis is the transverse coordinate axis along the spectrograph slit in CCD pixel numbers.

Finally, the delay created by the diffractive lens is obtained by comparing these two series of data and by taking into account the theoretical chromatism estimated for the refractive lens.

#78030 - $15.00 USD Received 12 December 2006; revised 17 January 2007; accepted 17 January 2007

The complete analysis of the interference pattern is made using a 1D-Fourier transform along the wavelength axis. Taking the expression of the fringes, the Fourier transform in the wavelength direction gives:

$$\tilde{I}(t,y) = FT\left[2A(\omega)\cdot A^{*}(\omega)\left[1+\cos(\omega\cdot\Delta\tau(y))\right]\right] \tag{21}$$

where $\Delta\tau$ is the delay given by Eq. (20).

$$\tilde{I}(t,y) = 2\cdot\tilde{A}(t)\otimes\tilde{A}^{*}(-t)\otimes\left[\delta(t)+\frac{\delta(t-\Delta\tau(y))}{2}+\frac{\delta(t+\Delta\tau(y))}{2}\right] \tag{22}$$

The Fourier transform of the signal for each Y coordinate presents a central peak and two satellites. The central peak contains information on the spectral shape of the pulses. The satellites contain information on the modulations of the spectrum. For our diagnostic, the satellite positions give information on the delay $\Delta\tau$ between the two replicas for each Y coordinate in the overlapping zone. Figure 11 shows the differences of the Fourier signals for a perfect and and for a chromatic beam. The satellite positions are not constant for a chromatic beam because of the variation of the delay along the Y coordinate.

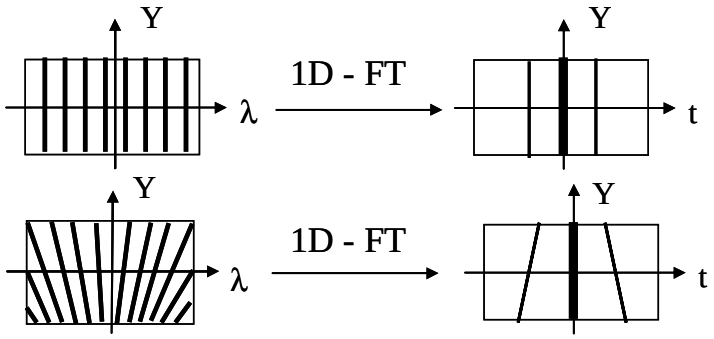

Fig. 11. Differences of the Fourier signals in the case of a perfect (top) and of a chromatic (bottom) beam. Due to the variation of the delay along the Y axis in the case of a chromatic beam, the satellite positions are not constant.

In Figs. 12 and 13 we plot the Fourier transform of the interference patterns of the two series of experiments shown in Figs. 9 and 10 respectively. The inversion of the tilt of the satellite locations induced by the diffractive Fresnel lens is visible.

#78030 - $15.00 USD Received 12 December 2006; revised 17 January 2007; accepted 17 January 2007

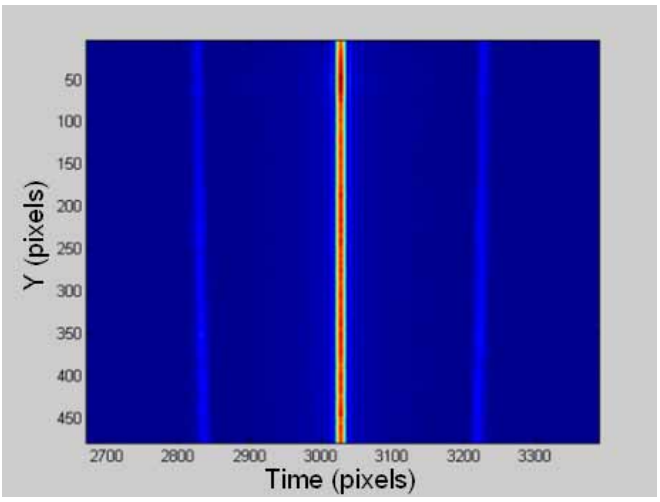

Fig. 12. Fourier transform of the interference pattern in the case of the refractive lens. A small variation of the satellite positions appears due to the chromatism accumulated in the Alisé chain, the refractive lens and in the diagnostic lenses. The horizontal axis is the delay axis in CCD pixel numbers. The vertical axis is the transverse coordinate axis along the spectrograph slit in CCD pixel numbers.

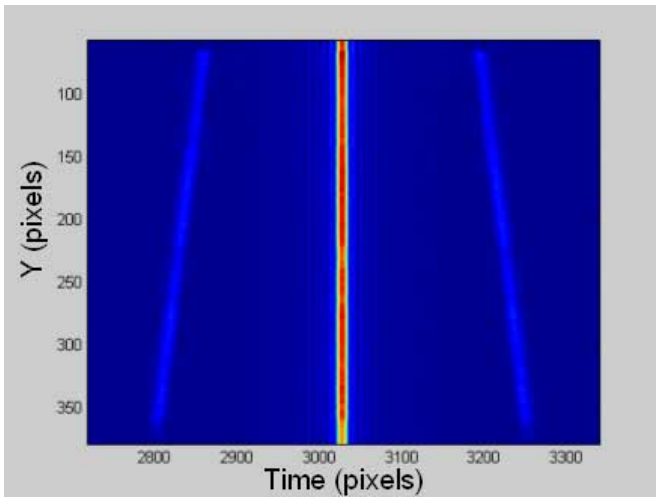

Fig. 13. Fourier transform of the interference pattern in the case of the diffractive lens. A strong variation of the satellite positions appears due to the chromatic aberrations of the diffractive lens. The horizontal axis is the delay axis in CCD pixel numbers. The vertical axis is the transverse coordinate axis along the spectrograph slit in CCD pixel numbers.

To extract the delay from these signals, three different calibrations are required. First, we need to calibrate the spectral response of the spectrometer. This is done using two lasers with different wavelengths: 1047 nm and 1053 nm. This calibration suppresses the T_r delay error that might come from a lack of parallelism between the spectrograph grating axis and the CCD X axis. Then, in order to estimate the spatial characteristics, the beam size (a) and the spatial shift (dy) in the interferometer must be measured. For these two points, a calibrated etalon aperture is inserted in the input pupil of the system near the lens aperture which is imaged with the spectrograph slit. In a first calibration measurement, an opaque mask is also inserted in one of the two interferometer arms. We calibrate this way the Y axis on the CCD. In a second calibration measurement, the opaque mask is removed and two separated images

#78030 - $15.00 USD Received 12 December 2006; revised 17 January 2007; accepted 17 January 2007

are recorded on the spectrograph CCD without overlapping, which allows us to calibrate the spatial shift: dy. These two spatial calibrations cancel the systematic error induced by a lack of parallelism between the slit direction, the shearing direction and the Y direction of the CCD.

Using these calibrations the slope of the satellite position variation, and, finally Eq. (19), the total delay measured is T_{r1} = 109 fs in the first experiment with the refractive lens and T_{r2} = -903 fs with the diffractive lens. The unique contribution of the diffractive lens T_{diff} is the difference between the two measurements (T_{r2} - T_{r1}) to which is added the estimated delay of the refractive lens T_{ref}. T_{ref} is calculated using Eq. (7) for a silica substrate and is equal to T_{ref} = 34 fs.

Finally, the diffractive lens introduces a delay T_{diff} = -978 fs for the 60 mm aperture, in good agreement with the specifications (1 ps). Moreover, with this interferometric single-shot diagnostic, we have measured the Alisé longitudinal chromatism to be 75 fs for a 60 mm aperture corresponding to 150 fs for the operating full beam aperture (85 mm). Again, this value for the Alisé chain is in good agreement with the calculation giving 183 fs.

4. Conclusion

We developed a self-referenced interferometric single-shot longitudinal chromatism diagnostic and used it to characterize a diffractive lens able to correct chromatism on Petawatt class lasers. Our measurements demonstrate that our diffractive lens delay is in good agreement with what we specified: a measured delay of 978 fs for a 1 ps delay specified. Being single shot, this measuring principle is well suited for high energy power chains like the PETAL facility. The potential of this diagnostic to realize spectrally resolved 1D-shearing interferometry has been pointed out and shall be detailed in a future work.

Acknowledgments

This work is supported by the Conseil Régional d'Aquitaine and is performed under the auspices of the Institut Lasers et Plasmas. We thank the Alisé facility for access and modular capabilities and the Alisé team, particularly C. Lepage, O. Bonville and E. Mazataud for their help in setting up the experiments, S. Montant from the CELIA laboratory for analyses of the experimental results, the LMO team (Optical Metrology Laboratory at CEA-CESTA) for the optical measurements on the 1.5 m Fresnel lens and H. Ward for the redaction.

#78030 - $15.00 USD Received 12 December 2006; revised 17 January 2007; accepted 17 January 2007